Available online at www.sciencedirect.com
SCIENCE DIRECT®
Continental Shelf Research 26 (2006) 733–751
CONTINENTAL SHELF RESEARCH
www.elsevier.com/locate/csr

Inter-annual variability in the timing of stratification and the spring bloom in the North-western North Sea

Jonathan Sharples[a,*], Oliver N. Ross[b], Beth E. Scott[c], Simon P.R. Greenstreet[d], Helen Fraser[d]

[a]*Proudman Oceanographic Laboratory, 6 Brownlow Street, Liverpool L3 5DA, UK*
[b]*Department of Biological Sciences, University of Essex, Colchester CO4 3SQ, UK*
[c]*School of Biological Sciences, University of Aberdeen, Aberdeen AB24 2TZ, UK*
[d]*Fisheries Research Services, Marine Laboratory, 375 Victoria Road, Aberdeen AB11 9DB, UK*

Received 23 September 2005; received in revised form 20 January 2006; accepted 30 January 2006
Available online 3 April 2006

Abstract

A physical–biological 1D numerical model, forced by tidal currents and observed meteorology, has been used to simulate the inter-annual changes in the timing of spring stratification and the spring phytoplankton bloom between 1974 and 2003 in the Marr Bank region of the North-western North Sea. The model successfully simulated the observed long-term variability and warming trend of water temperatures in the region, indicating that the oceanographic climate is influenced primarily by local meteorology rather than by inflows of water from the NE Atlantic Ocean. The spring-neap tidal cycle is shown to affect the timing of the onset of stratification and the spring bloom, with established spring stratification usually beginning as tidal currents decrease from springs to neaps. Spring-neap tidal variability can also produce double spring blooms when stratification that develops after a neap tide is temporarily broken down by the increasing tidal mixing towards the next spring tide. Over the 30 years of model simulations the dominant meteorological control on the timing of the spring stratification and bloom was the spring air temperature. However, there is evidence that control by wind stress variability on the timing of spring stratification was more important before the early 1990s ($r^2 = 0.32$, significant at 95%). After the early 1990s the wind stress was not significantly correlated with the timing of spring stratification, and the spring air temperature became the main control ($r^2 = 0.33$, significant at 95%). Increasing air temperature also appears to have driven a gradual trend in the timing of stratification and the spring bloom since the mid 1990s of an average 1 day earlier per year ($r^2 = 0.27$, significant at 95%). The link between the spring meteorology and the North Atlantic Oscillation (NAO) was investigated, indicating that the NAO played a role in the timing of stratification and the spring bloom prior to 1990, with a significant correlation between the NAO and the spring wind stress, but has had less of a role since 1990, with only a weak connection between the NAO and the spring air temperature.

Keywords: Spring bloom; Thermal stratification; Mixing processes; Inter-annual variability; Modelling; Europe–North Sea–North-western North Sea–Marr Bank

*Corresponding author. Tel.: +44 151 795 4800.
E-mail address: js1@pol.ac.uk (J. Sharples).

0278-4343/$ - see front matter © 2006 Elsevier Ltd. All rights reserved.
doi:10.1016/j.csr.2006.01.011

1. Introduction

Phytoplankton growth in temperate seas is often closely dependent on the spring development of water column stability, providing a well-lit surface layer for the rapid spring bloom (Sverdrup, 1953; Pingree et al., 1977). This production during the spring bloom can be an important source of organic fuel for much of the pelagic and benthic food chains (Townsend and Cammen, 1994; Verity et al., 2002). Overall the spring primary production can contribute as much as a third of the total annual primary production in a shelf region (e.g. Townsend et al., 1994), often taking place in a time as short as 1 or 2 weeks. The timing of the bloom has been seen to impact on the success of copepods (e.g. Melle and Skjoldal, 1998; Head et al., 2000). Both phytoplankton and copepods form the diet of many larval fish, and the timing of the spring bloom of phytoplankton influences the survival of juvenile fish (Platt et al., 2003), interpreted in terms of the concept of "match–mismatch" between bloom timing and larval development (Cushing, 1982). As the precursor to the spring bloom, the timing and extent of water column stratification thus play pivotal roles in seasonal cycles of biology in shelf seas. Understanding the causes of inter-annual variability in the timing of the onset of stratification and the spring bloom is thus a key requirement in developing a broader understanding of ecosystem variability.

In the open ocean the timing of the spring stratification is determined principally by the timing of the shutdown of convective over-turning. Episodic surface wind stress then adds "noise" by adding mixing energy and potentially delaying the onset of stratification (Waniek, 2003). In temperate shelf seas, away from sources of freshwater, the development of stratification is controlled by the competition between the stratifying influence of surface solar irradiance, and the competing mixing driven by tidal currents, surface wind stress, and convective over-turning (Simpson and Hunter, 1974; Loder and Greenberg, 1986). In tidally-energetic regions, such as the shelf seas of NW Europe, North-eastern North America, and the Patagonian shelf, tidal mixing plays a particularly important role in determining the summer vertical water column structure (Simpson, 1981; Loder et al., 1993; Glorioso and Simpson, 1994). Compared to the open ocean, this addition of strong tidal mixing will be expected to delay the start of stratification as the solar elevation has to increase further into spring before the rate of heat supply to the sea surface can counter the mixing supplied by both wind and tide. Viewing the tides as providing a persistent "background" level of mixing, the more episodic meteorological forcing could again be seen as controlling the inter-annual variation in the time at which stratification begins. A more detailed inspection of the tidal mixing has suggested a role for the spring-neap cycle off Georges Bank, with transient stratification events associated with the brief period of low mixing at neap tides (Bisagni, 1998).

Developing our understanding of how the ecosystem responds to the inter-annual physical variability in shelf seas requires long-term data on primary production and water column structure. Relatively short term time series are now available from the satellite imagery (e.g. Follows and Dutkiewicz, 2002). Much longer-term observations are provided by the continuous plankton recorder (CPR), which have for instance indicated significant changes in the seasonal pattern of surface chlorophyll in the North Sea and Atlantic Ocean (Reid et al., 2001b). Long-term applications of numerical models are particularly suited to investigation of the precise timing of stratification and the spring bloom, though most have been applied in 3D to investigations of inter-annual variations in primary production (e.g. Moll and Radach, 2003).

Our approach is to use a 1D (vertical) numerical model, driven by a 30-year time series of meteorological observations, in the North-western North Sea. Our study area is offshore of the Firth of Forth, over the Marr Bank (Fig. 1). This is an important area for sandeels and breeding seabirds (e.g. Proctor et al., 1998; Furness and Tasker, 2000), and quantifying the long-term variability of the spring stratification and bloom is a key component in the understanding of ecological mechanisms behind variations in marine animal populations which are responding both to climate changes and the activities of industrial fisheries (e.g. Frederiksen et al., 2004).

While the 1D approach is simpler to implement and computationally cheaper than the 3D shelf models, it is important to determine that the environment under investigation is adequately simulated by considering vertical processes only. The North-western North Sea is tidally-energetic and moderately deep, and undergoes thermal stratification in the late spring and summer as the solar heat supply exceeds the combined mixing

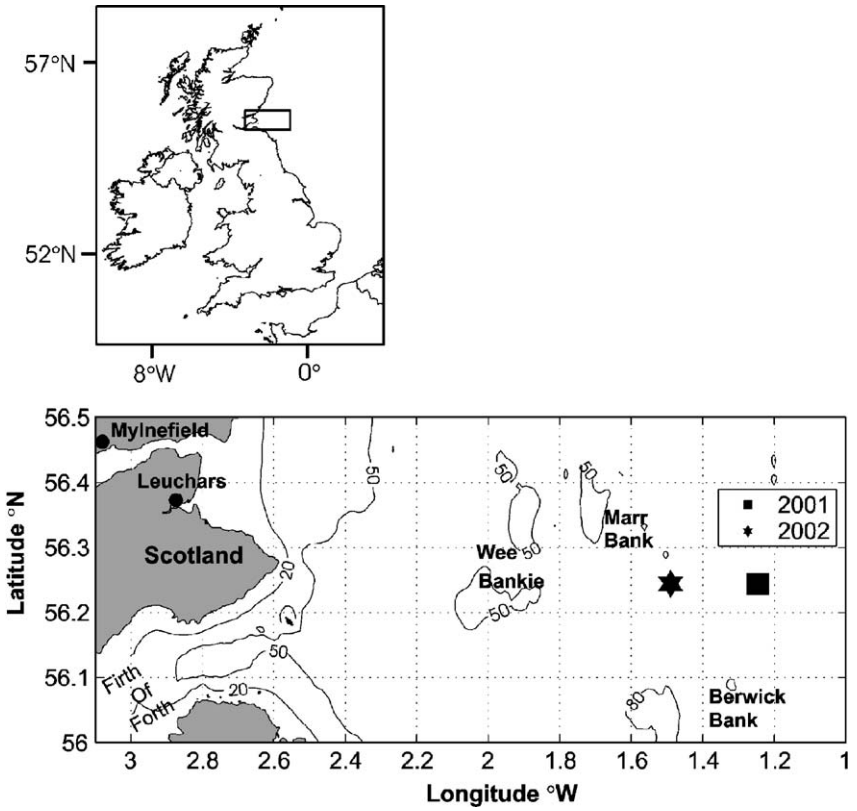

Fig. 1. Map of the mooring sites and positions of weather stations used for meteorological data.

influences of tide and wind (Rodhe, 1998). However, in addition to this vertical interaction between meteorological forcing at the sea surface and the tidal mixing, the northern North Sea is also influenced by exchange with the Northeast Atlantic Ocean. This exchange occurs primarily to the east of the region through the Norwegian Trench (Turrell et al., 1992), but also via the Fair Isle and East Shetland currents (Turrell, 1992). Inflow via the Fair Isle Current is thought to be confined in the northern North Sea by the 100 m isobath (Turrell et al., 1992). Comparison between a 1D model and long-term temperature data throughout the North Sea has shown that advection only plays a significant role in the far north and north–east (Norwegian Trench) of the North Sea (Elliott and Clarke, 1991). However, satellite observations have been used to infer advection as an important control on the inter-annual variability of North Sea temperatures (Reid et al., 2001a). Part of our model validation will demonstrate that, in the region of our mooring deployments in the North-western North Sea, the inter-annual variability in temperature is almost entirely attributable to vertical air-sea and mixing exchange processes.

We address the following specific questions:

(1) How variable is the timing of the onset of water column stratification and the spring bloom, and are there any significant trends?
(2) What are the important factors in generating inter-annual variability in the timing of stratification and the spring bloom?
(3) Is the variability of stratification and the spring bloom linked to larger-scale climate variability (i.e. the North Atlantic Oscillation)?

In the following Section 2 we describe the numerical model. In Section 3 we describe the calibration and validation of the numerical model, using both short term and long-term data sets, and including an assessment of the applicability of the 1D approach to the north-western North Sea. In Section 4 the basic results are shown, and Section 5 provides answers and discussion for the questions listed above.

2. Method

The main question to be addressed requires the modelled phytoplankton to respond to the physical environment in spring, as the water column ceases to convectively over-turn and heat input begins to play a role in controlling vertical fluxes of biomass and nutrients. We focus on the use of a relatively sophisticated physical model to track the changes in the temperature and turbulence structure of the water column as accurately as possible. We do not attempt to simulate inter-annual variability in the detailed biochemistry, but instead use a simple biological model that allows us to investigate the potential inter-annual variability in the response of the primary producers to the changes in physical forcing in late spring and early summer. The model is described below, with the details of the model equations shown in Appendix A.

The 1D (vertical) numerical model is similar to that presented in Sharples (1999), simulating vertical profiles of currents, temperature, turbulent mixing, phytoplankton biomass, and dissolved inorganic nitrogen. The physical component of the model is forced by an oscillating sea surface slope with five tidal constituents (M2, S2, N2, O1, K1), driving the tidal currents (Eqs. (A.1), (A.2)). A quadratic friction boundary condition at the seabed generates vertical shear of the currents. Heat fluxes across the air–sea boundary are controlled by a formulation requiring surface solar irradiance, wind speed, air temperature, atmospheric pressure, relative humidity and cloud cover (Eqs. (A.10)–(A.15)). A quadratic stress boundary condition at the sea surface transmits wind-driven momentum into the water column. Vertical frictional coupling of momentum and vertical turbulent diffusion of scalars are controlled by a k–ε turbulence scheme (Canuto et al., 2001; Eqs. (A.17)–(A.27)). A parameterisation for internal wave mixing at the thermocline is included following Large et al. (1994) (Eqs. (A.28)).

Accurate tidal and meteorological forcing are critical to the success of the model. The tidal constituent amplitudes of the oscillating sea surface slope were calculated using tidal current measurements from a current meter mooring (see Section 3.1) and assuming that the surface current measurements were outside of the bottom boundary layer (Sharples, 1999). Meteorological observations were available as daily means from two weather stations: Leuchars (56.377°N, 2.861°W) and Mylnefield (56.458°N, 3.072°W) (Fig. 1). These sites were chosen because of their close proximity to the coast, and also as both are surrounded by low-lying land. The model simulated diurnal variability of the surface incident irradiance by distributing the mean daily irradiance over a half-sinusoid between sunset and sunrise, with the time between sunrise and sunset calculated as a function of latitude and day through the year. The available daily mean wind data consisted of mean wind speed and direction, along with the standard deviations of wind speed and direction about their daily means. To account for this variability in wind stress during the day, hourly variability of the wind speed and direction were modelled by randomly sampling a Gaussian distribution centred on the means and with width governed by the standard deviations.

The biological model is a cell quota, threshold limitation model (Tett, 1987; Sharples and Tett, 1994) simulating vertical profiles of phytoplankton biomass and dissolved inorganic nitrogen. With the focus on the initial stages of the spring bloom, the phytoplankton parameters are set to be representative of a diatom (Tett, 1987). Biomass is modelled as chlorophyll, with a fixed C:chl ratio. Growth occurs in response to the two potentially-limiting resources of light and dissolved inorganic nitrogen; if either the light environment or the phytoplankton internal nutrient quota is insufficient for growth, then the phytoplankton respire. Phytoplankton are grazed using a fixed grazing rate acting on the phytoplankton biomass. The grazing rate used is a typical value for spring/early summer in the northern North Sea (Lee et al., 2002). We do not attempt to model the seasonality of the grazing rate. An important consequence of this is that the modelled decay of the spring bloom is unlikely to be as sharp as reality and thus we do not attempt any quantitative interpretation of post-bloom results from the model. A fraction of the grazed cell nutrients are assumed to be recycled immediately back into the dissolved inorganic nitrogen. Phytoplankton biomass (including the internal cell nutrients) and the surrounding dissolved inorganic nitrogen are mixed vertically by the turbulence calculated by the physical component of the model. There are no fluxes of phytoplankton through either of the model boundaries, while remineralised nitrogen diffuses from the seabed into the bottom model grid cell to replenish the water column nutrients towards a fixed concentration. The modelled region of the North-western North Sea is away from the influences of nutrient supply from either rivers or the shelf edge.

3. Model calibration and validation

3.1. Model comparison with short term mooring data

A current meter and temperature logger mooring was deployed south of the Marr Bank (mean depth = 60 m; Fig. 1) in 2001 and 2002. Near surface current information from the 2002 mooring deployment was harmonically analysed for the M2, S2, N2, O1, and K1 tidal constituents (Table 1). The amplitudes and phases of the tidal current constituents were then used to calculate the amplitudes and phases of the oscillating sea surface slope required by the model. A similar harmonic analysis of the 2001 current data simulated by the model indicated satisfactory agreement with the observed tidal currents (Table 1), with the most significant constituent amplitudes being modelled to within $0.01\,m\,s^{-1}$, and their phases to within 30 min.

The most complete dataset of temperature information, collected by the 2002 mooring deployment, was used to calibrate the model. The full set of model driving parameters resulting from calibration against the 2002 mooring data is included in Appendix A (Table A1). The model-observation comparison of the onset of stratification (Fig. 2) for the 2002 mooring deployment shows that the model correctly simulated both the onset of the main seasonal stratified period on about April 30th, and a short period of weak stratification in late April. It is clear that the timing of the return to complete vertical mixing was more difficult to model, with the simulated temperature structure returning to a vertically mixed state 20 days after the observed date of September 23rd. This appears to be due to a failure of the modelled bottom temperature to track the slow warming observed from early July. At the same time that the observed bottom temperatures began to warm compared to the model simulation, the observed bottom temperatures also began to show significant semi-diurnal variability. This indicates a local horizontal gradient in bottom layer temperature, with advection of this temperature gradient by non-tidal residual flow resulting in the observed temperature increase. Advection of warm oceanic water from the shelf edge is unlikely. The mean bottom water current observed at the moorings during the warming in summer was typically $1–2\,cm\,s^{-1}$ southward, in agreement with surface drifters that have been observed to travel from the shelf edge to at least as far south as 57°N (Burrows et al., 1999). Assuming such a velocity was maintained, the fastest transit time for oceanic water between the shelf edge and the Marr Bank region would be approximately 1 year. It is unlikely that the Atlantic water could maintain its temperature signature on such a long journey across the shelf. A more likely source of the warmer bottom water at the mooring site is the relative warming of the thinner bottom layer over the Marr Bank just to the north of the mooring which is then brought to the mooring by the weak southward mean flow.

In the context of the objectives described in the introduction an inability to simulate the timing of autumnal re-mixing is not a serious failure. The weak southward flow observed, and the lack of any significant horizontal temperature gradients in winter and spring, mean that the 1D approach to modelling the onset of spring thermal stratification is valid. The key success of the model is this ability to simulate correctly both the initial period of weak stratification, and the onset of the sustained seasonal stratification. This ability is confirmed by comparing the calibrated model against the independent data set provided by the mooring deployment in 2001. The 2001 mooring was less successful than 2002, as a result mainly of instrument damage and loss in collisions with (we assume) shipping.

Table 1
Comparison of tidal constituents from the 2001 mooring observations and the model, showing the close agreement between predicted and observed tidal currents

Tidal constituent	Observed along-shore amplitude ($m\,s^{-1}$)	Modelled along-shore amplitude ($m\,s^{-1}$)	Observed-modelled along-shore phase discrepancy (min)	Observed cross-shore amplitude ($m\,s^{-1}$)	Modelled cross-shore amplitude ($m\,s^{-1}$)	Observed-modelled cross-shore phase discrepancy (min)
M2	0.34	0.33	29	0.06	0.09	−56
S2	0.14	0.13	22	0.03	0.04	−26
N2	0.06	0.06	28	0.01	0.02	−82
O1	0.03	0.04	−22	0.00	0.00	−212
K1	0.03	0.03	−27	0.00	0.00	−72

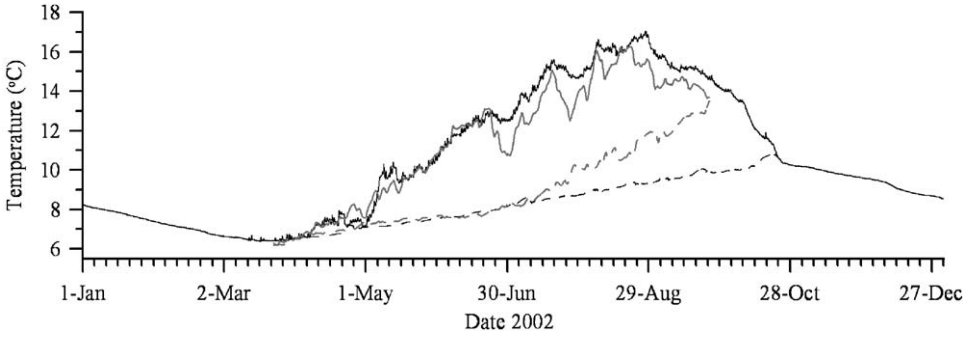

Fig. 2. Comparison between observed and modelled temperatures at the mooring site in 2002. Solid lines are near-surface and dashed lines are near-bed. The black lines are the model prediction, the grey lines are from the mooring observations. The model was calibrated against this 2002 mooring data.

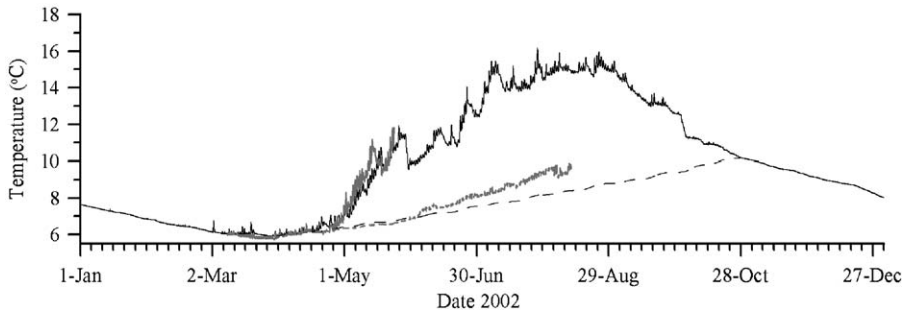

Fig. 3. As Fig. 2, but for validation of the model against the 2001 observed temperatures. Model driving parameters were the same as the calibrated 2002 model run shown in Fig. 2.

However, enough near-surface and nearbed temperature data exist to show that the model is able to simulate correctly the onset of stratification in late April 2001 (Fig. 3). The process of bottom layer warming after stratification has become established is again apparent in the observations though is not as strong as in 2002.

3.2. *Long term model behaviour compared to observations*

Ideally the model should be able to run reliably for the full 30 years of meteorological data available without any further calibration. A failure of the model to simulate the long-term temperature behaviour could indicate that the advection of NE Atlantic inflows makes an important contribution to the temperature of the Marr Bank region and we would question the utility of the 1D model approach. A long-term data set for the North Sea, held by the International Council for the Exploration of the Sea (ICES), provided monthly mean surface and bottom water temperatures suitable for assessing the model's long-term behaviour. These observations were extracted for positions within an area covering the Marr Bank mooring (bounded by $\pm 1.0^{\circ}$ latitude and $\pm 0.5^{\circ}$ longitude around the 2002 mooring position). The size of the sampled area was determined by the need to acquire enough data points to cover adequately the entire 30 years of model simulation, while the area was designed to avoid the influence of low salinity coastal waters. Data were extracted, when available, for each month between 1974 and 2003. The temperature time series was complete for every February between 1974 and 2003, providing an ideal data set for model assessment. Salinity data was also extracted from the ICES database. The time series of monthly bottom-surface salinity differences in the vicinity of the mooring was used to confirm that temperature was the dominant control on stratification in the Marr Bank region (not shown). Initially it was hoped that a time series of winter nitrate data could be used to control the pre-bloom

concentration of dissolved inorganic nitrogen in the model (S_b in Table A1). However, reliable nitrate data was only available after 1986 and so the model was run with the mean value observed in the winters 1986–2003. Thus only the timing of the spring bloom can be interpreted in the model results; inter-annual variability in the magnitude of the bloom will be controlled strongly by variability in the pre-bloom nitrate concentration.

The model was run continuously for the entire 30 years, and a comparison made between the model results and the ICES data (Fig. 4). Time series of February water temperatures (Fig. 4a) shows model and ICES data to be very strongly correlated ($r^2 = 0.80$), with modelled temperatures tracking the variability of the observations remarkably well. In particular, the increases in mean winter temperature of the North Sea that occurred over the late 1980s and late 1990s (e.g. Holliday and Reid, 2001) are clear in the ICES data and are correctly simulated by the model. The mean annual rate of change of winter temperature produced by the model ($0.05 \pm 0.01\,^{\circ}\mathrm{C\,a^{-1}}$) is consistent with that from the ICES observations ($0.04 \pm 0.01\,^{\circ}\mathrm{C\,a^{-1}}$), with the de-trended data showing the model to capture 71% of the observed inter-annual variability. With the mean discrepancy between the model and the ICES observations of February temperatures being $-0.1 \pm 0.3\,^{\circ}\mathrm{C}$, the only year when the model deviates significantly from the observations was 1989 when the modelled temperature was $0.9\,^{\circ}\mathrm{C}$ less than the observations. The observed warmer water could indicate an Atlantic inflow event not captured by the model. However, the ICES salinity data for the same region does not show any significant departure from the long-term mean; for an inflow event we would expect a warm, salty anomaly. A more detailed comparison of all of the available monthly mean surface and temperature data in the ICES database shows that the model successfully reproduces the seasonal and inter-annual variability in surface temperatures (Fig. 4b). Comparison of bottom water temperatures again shows a strong correlation (Fig. 4c), though the model tends to under-predict the warmer (i.e. late summer) bottom water temperature, consistent with the late summer advection of heat into the region identified in the current meter mooring records. Despite this influence of local advection during summer, the long-term agreement seen in the

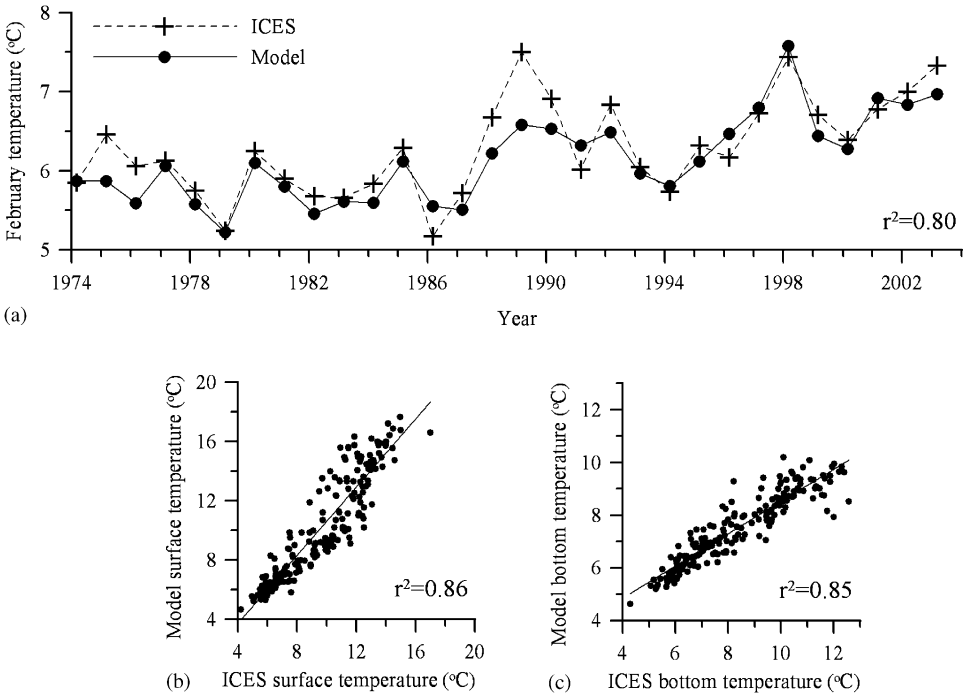

Fig. 4. Model comparison with ICES observed temperature data between 1974 and 2003: (a) mean water temperatures in February of each year; (b) correlation between model and ICES data of all mean monthly surface temperatures; and (c) correlation between model and ICES data of all mean monthly nearbed temperatures. Note the good agreement in modelled winter temperatures (a). Warmer temperatures modelled in summer ((b) and (c)) show more deviation from observations.

comparison of winter temperatures shows that winter convective over-turning is very effective at equilibrating the water column temperature to local meteorological conditions. This again shows that an Atlantic temperature signal is unlikely to survive the 12 month journey from the shelf edge to the Marr Bank region (e.g. Elliott and Clarke, 1991).

4. Results

Between 1974 and 2003 the model results show that the onset of sustained stratification occurs typically around Julian Day 111 (April 21st), with a range of approximately ± 3 weeks either side (Fig. 5, Table 2). Short-lived periods of weak stratification occur as early as late March. The net heat flux becomes positive into the sea surface at a mean date of March 15th, and varies between February 13th and April 3rd (Table 2). The onset of the main period of stratification in Table 2 is defined as the first date after which the surface-bottom temperature difference exceeds 0.5 °C and is maintained for at least 3 days, preventing earlier short-term stratification events being identified as the beginning of the main summer stratification. Such short events tend to be diurnal, caused by a day of bright sunlight but then convectively removed during the next night. They are too short for the primary producers to respond to significantly. Not surprisingly the thermal stratification never occurs before the establishment of net heat flux into the sea surface. The timing of the onset of stratification can be anywhere from a few days to over 2 months after the establishment of net heat supply into the sea. The smaller delays are associated with later timing of the onset of net heat supply. The mean delay of about 1 month represents the additional heating required to overcome the influence of the tidal mixing. This can be confirmed by noting that the mean heat flux supplied to the sea surface in the 30 days after March 15th is $20\,\mathrm{W\,m^{-2}}$. Using the analysis of Simpson (1981), the influence of this heating in stratifying the water column can be offset by a tidal current amplitude of $0.4\,\mathrm{m\,s^{-1}}$. This is indeed the effective mean tidal current amplitude that results in the same long-term average mixing rate generated by the six tidal constituents used by the model.

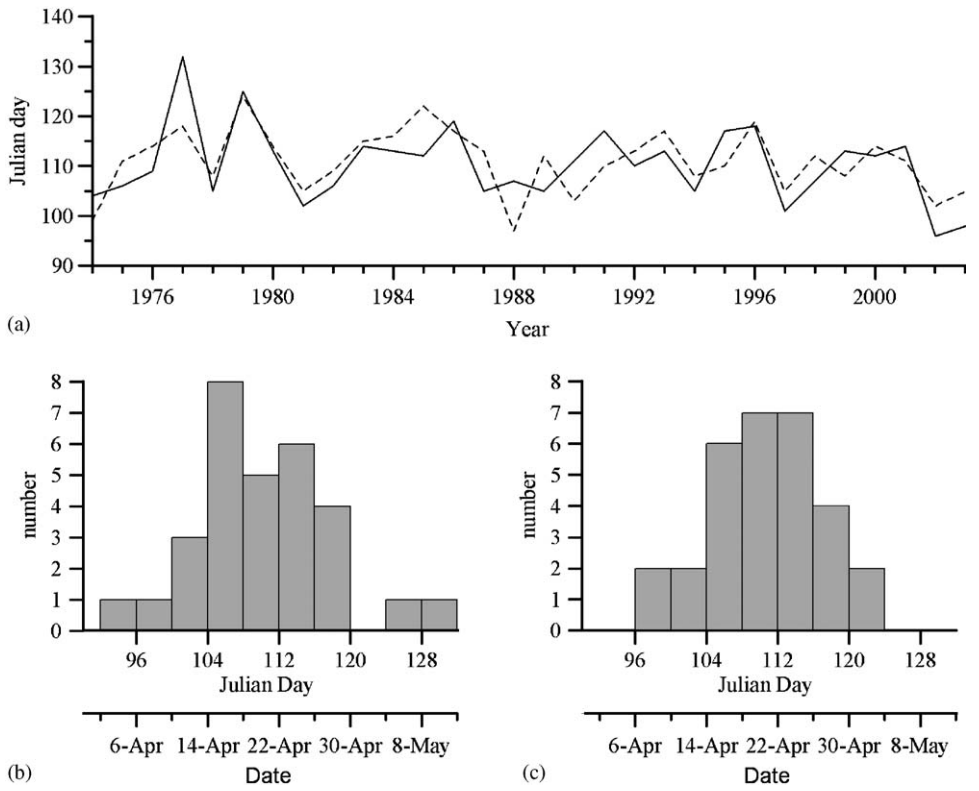

Fig. 5. (a) Modelled timing (Julian days) of the spring stratification (solid line) and spring bloom (dashed line) between 1974 and 2003; (b) distribution of the modelled timing of spring stratification; and (c) distribution of the modelled timing of the spring bloom.

Table 2
Statistics of stratification and bloom timings

Event	Mean	Earliest	Latest	Variance (d^2)
Onset of net heat flux into sea surface	15th March	13th February	3rd April	100
Onset of thermal stratification	20th April	6th April	12th May	64
Onset of the spring phytoplankton bloom	21st April	7th April	4th May	36

The start date of the spring bloom was identified by noting the timing of the maximum daily rate of change of surface biomass in spring. The mean modelled start date for the bloom was April 22nd, and varied only between April 8th and May 5th (Table 2). The onset of the spring bloom was less variable than the onset of stratification (Fig. 5, Table 2), primarily because the latest bloom date occurs one week before the latest date for stratification. In two years, 1988 and 1990, the bloom appears to begin well before the identified time of spring stratification. In both cases the growth is in response to a short period of weak stratification that does not fit the criteria used for the onset of spring stratification. The smaller range of dates of the bloom onset compared to the onset of stratification is a result of the fixed physiological characteristics of the modelled phytoplankton. In late spring the phytoplankton are able to respond to the increasing irradiance through the whole water column without the development of near-surface stability. Within the shallow water around Marr Bank, and taking the phytoplankton parameters as a suitable set for a real species, it would be reasonable to expect the bloom to occur in late spring in the absence of stratification.

There is no statistically significant trend in either the stratification or bloom timing over the 30 years (Fig. 5a). However, there is evidence of greater variance in the timings prior to 1990 and an indication of earlier timings developing in the late 1990s and early 2000s. Between 1991 and 2003 there is a weak trend in the onset of stratification, with the date becoming earlier by approximately 1 day per year ($r^2 = 0.27$, $n = 13$, significant at 95%).

A closer look at the spring bloom timing (Fig. 6) shows that some years exhibit a significant double peak in chlorophyll as the bloom starts, with surface chlorophyll being rapidly redistributed through the water column shortly after the onset of the bloom and then recovering to bloom concentrations a few days later. Particularly strong examples of this phenomenon are modelled for 1978, 1983, 1986, and 1997. Less pronounced examples are 1975, 1988, and 1996. In each of these examples the initial bloom is triggered by stratification developing at or close to a neap tide, with subsequent re-mixing occurring at the next spring tide.

5. Discussion

The following discussion will focus on four key aspects of the results towards answering the original objectives: (1) the successful hindcasting of winter temperatures by the model and the implications for the influence of Atlantic inflows, (2) the contribution of spring-neap tidal variability to the timing of stratification and the spring bloom, (3) the role of meteorology in driving inter-annual variance and trends in the timing of stratification and the spring bloom, and (4) the influence of the North Atlantic Oscillation (NAO) on the spring meteorology.

The comparison between modelled and observed temperatures over the 30 years showed a remarkable agreement, with 80% of the observed inter-annual variance in winter temperatures captured by the numerical model (Fig. 4). Given that the model only includes meteorology and vertical exchange within the water column, and does not have any formulation for advective flows, its success shows that the source of warmer water in the North-western North Sea is local meteorological forcing, rather than inputs of warmer water from the North Atlantic. In the one year when there was a model-observation discrepancy possibly related to Atlantic inflow (1989), the possibility of an inflow event was not supported by the salinity observations. Elliott and Clarke (1991), and Prandle (1998), have demonstrated that much of the seasonal variability in the temperature structure of the North Sea is dominated by meteorological fluxes and vertical mixing. Our work has shown that this is also true, at least in the Marr Bank region, on decadal time scales. This has particular importance for the interpretation of, for instance, population fluctuations in communities that depend on over-wintering water temperatures

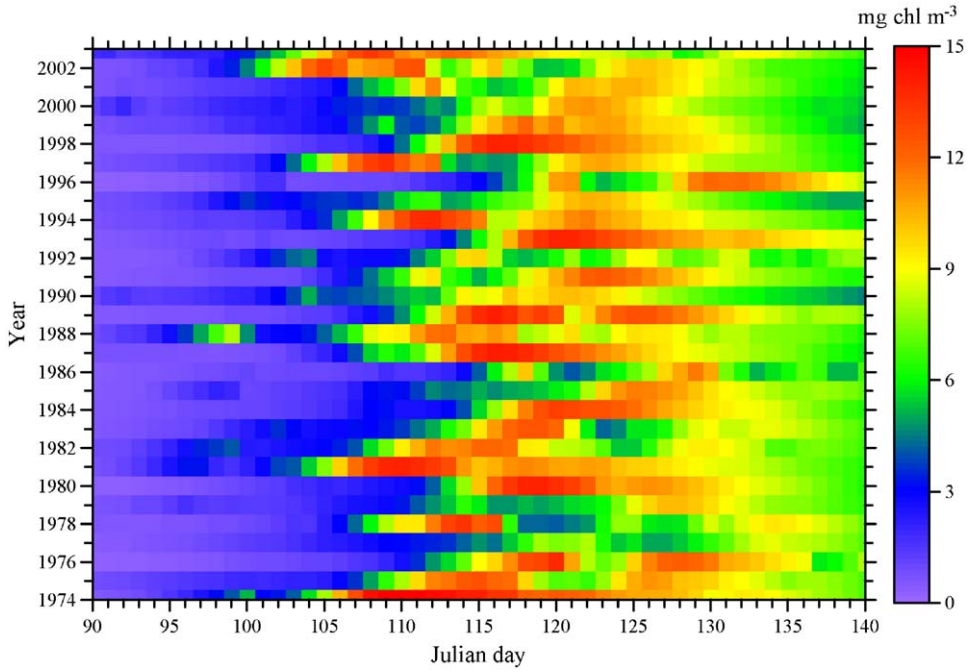

Fig. 6. Spring changes in modelled surface chlorophyll between 1974 and 2003. Strong "double bloom" responses to the spring-neap cycle of tidal mixing occurred in 1978, 1983, 1986, and 1997.

and on the timing of the spring thermal stratification (e.g. the Marr Bank sandeels and the seabird colonies of eastern Scotland and north-eastern England). Note that this result only applies to water temperature, probably because the slow mean transport rates of Atlantic water from the shelf edge allow the water to reach a balance with local meteorology. Direct evidence for North Atlantic water entering the North Sea needs to be sought in other parameters that may have signals with a longer lifetime (e.g. salinity or nitrate; Svendsen and Magnusson, 1992).

The model results showed that the spring-neap cycle of tidal mixing can lead to temporary re-mixing of an established bloom. Taking 1983 as an example (Fig. 7a) illustrates how the low mixing of approaching neap tidal currents (23rd April 1983) can allow the onset of stratification and the associated response of the near-surface phytoplankton. The next spring tide is, however, strong enough to mix the stratification as well as counter the increasing rate of surface irradiance. As the water column is briefly mixed, the surface biomass is redistributed through the entire water column (6th May), with about 70% of the bloom biomass being trapped below the new thermocline that develops approaching the next neap tide. Such a marked double pulse of the surface productivity may have consequences for the rest of the marine community. Bisagni (1998), reports similar neap-tide stratification events on Georges Bank. This transient stratification on Georges bank is correlated with the maximum abundance of cod larvae, while the development of the more established spring stratification is linked to the maximum abundance of haddock larvae.

The double spring blooms are the most obvious result of the spring-neap tidal cycle. However, there is a more general effect on the timing of spring stratification that is highlighted by considering the timing of stratification as a function of the phase within the spring-neap cycle (Fig. 8). In 22 of the 30 years the spring stratification is predicted to have begun either at neap tides or as the tidal currents decreased from spring to neaps, indicating that the low mixing immediately following the onset of stratification is important in allowing the stratification to become strongly established. Stratification began at spring tides or as the tides increased from neaps to spring in eight of the thirty years. For the years when stratification began close to spring tides, weather conditions aided the stratification with low winds and strong irradiance, with the subsequent reduction in tidal mixing towards the next neap tide

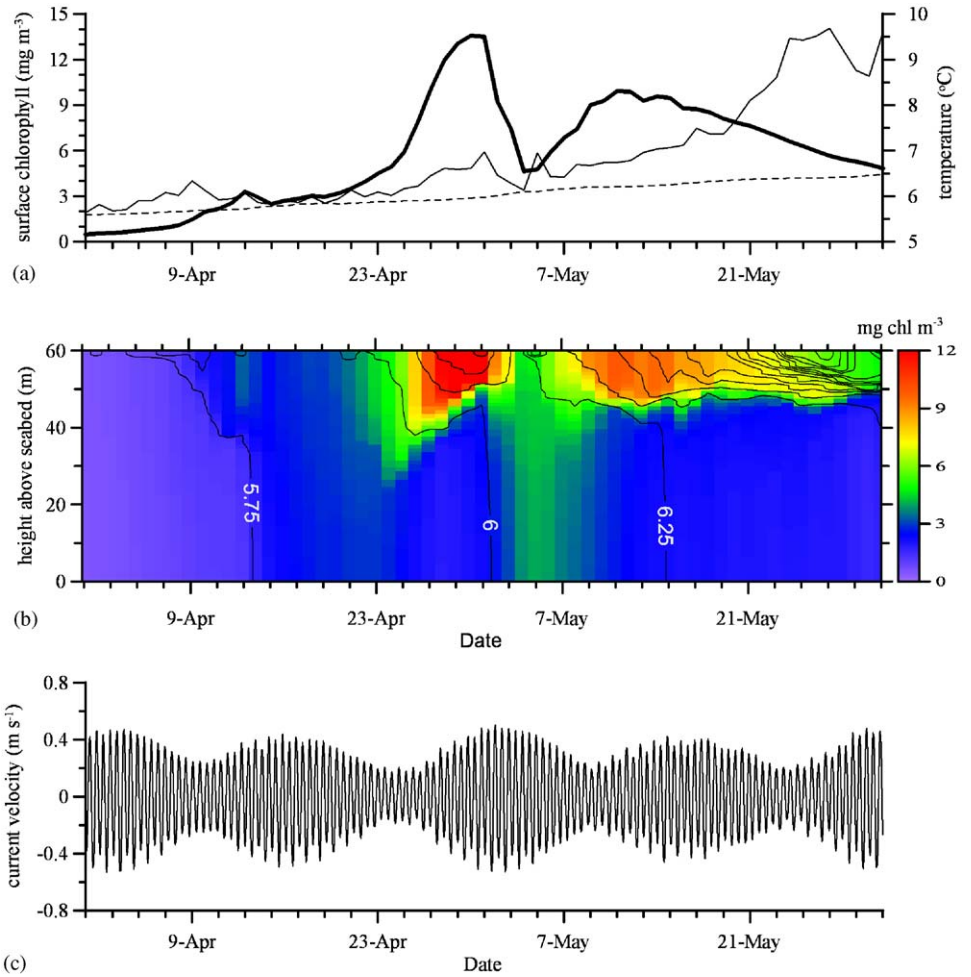

Fig. 7. An example of the effect of the spring-neap cycle on the stratification and bloom in spring 1983, illustrating the vertical structure of the double bloom driven by the re-mixing of stratification by a spring tide: (a) modelled surface (thin line) and bottom (dashed line) temperatures and surface chlorophyll (bold line); (b) modelled vertical distribution of chlorophyll (colours) and temperature (lines, contoured every 0.25 °C) through spring. The spring tide of May 3rd mixes the initial stratification and the products of the first spring bloom throughout the water column; and (c) modelled tidal currents along the major axis of the tidal ellipse showing the spring-neap cycle.

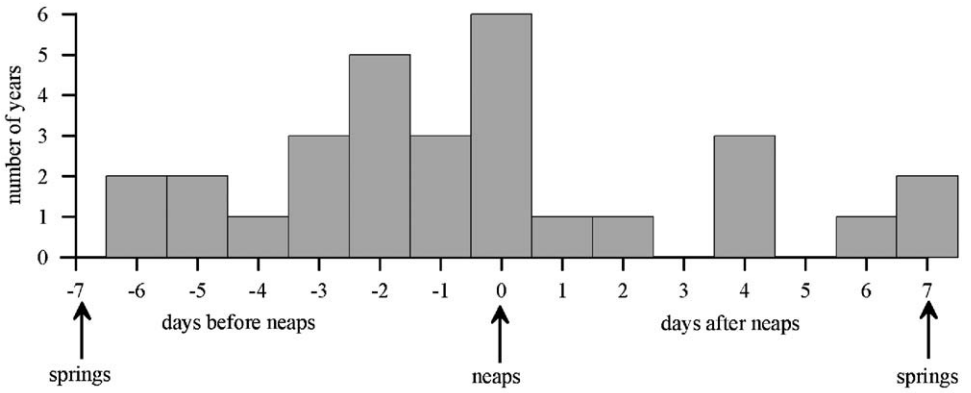

Fig. 8. The distribution of the modelled spring stratification events between 1974 and 2003 relative to the timing of the spring-neap cycle. In 75% of the years established stratification begins as tidal currents decrease from spring to neap tides.

further allowing the stability to become established. For the three years when stratification began 4 days after neap tides, i.e. at the time of the maximum rate of increase of the tidal mixing, stratification was maintained towards the spring tide but was only weak; stratification did not strengthen until after the spring tide. Finally, for the two years when stratification began shortly after neap tides it appears that there is a 1–2 day window after neaps when the tidal mixing is increasing slowly and enough stratification can develop sufficiently to counter the mixing of the next spring tide. This identification of this spring-neap control on the timing of stratification has the potential to be a useful tool in the prediction of spring bloom timing in tidally energetic shelf seas.

Given the importance of the meteorological forcing to the evolution of temperature and stratification it is worth considering if there are any dominant meteorological parameters in spring that drive most of the variability. The inter-annual variability of the timing of stratification and the spring bloom was correlated with the mean spring (March to May) values of wind stress, solar irradiance, air temperature, air pressure, and relative humidity. Over the whole 30 years the only significant correlation was with the air temperature (negative correlations of $r^2 = 0.21$ and $r^2 = 0.28$ for

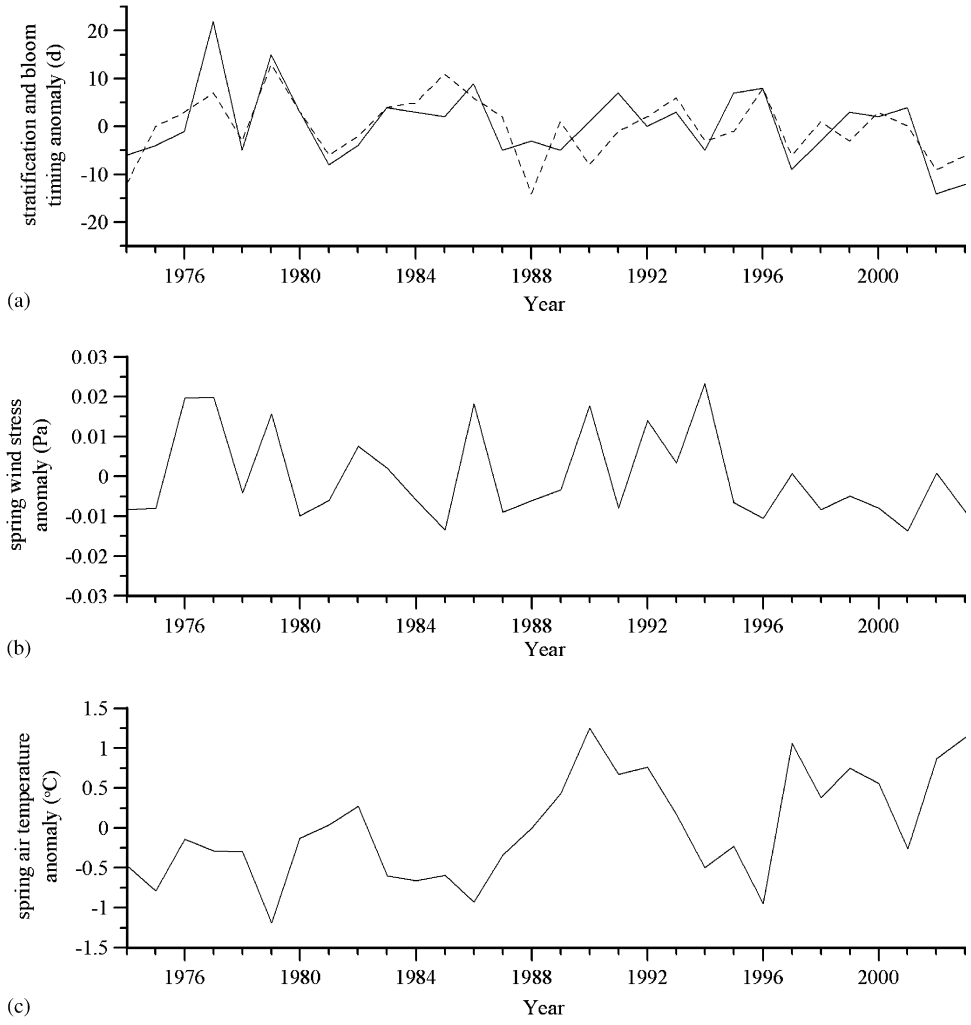

Fig. 9. (a) Modelled timing (Julian days) of the spring stratification (solid line) and spring bloom (dashed line) between 1974 and 2003 relative to the mean; (b) time series of the average spring wind stress, relative to the 1974–2003 mean; and (c) time series of the average spring air temperature, relative to the 1974–2003 mean. Only the spring air temperature anomaly is significantly correlated with the stratification timing over all 30 years. Stratification timing is significantly correlated with the spring wind stress anomaly between 1974 and 1990.

stratification and bloom timing respectively, both significant at 99%). Thus the date of stratification and the spring bloom becomes earlier during warmer springs. Not surprisingly, given the requirements of photosynthesis, the timing of the spring bloom was also correlated with changes in the mean spring solar irradiance ($r^2 = 0.19$, significant at 95%). The lack of a significant correlation with the spring wind stress is perhaps unexpected, as we would normally expect changes in surface mixing to play a role in controlling the development of thermal stratification. A more detailed consideration of the 30 years of spring wind stress and air temperature provides an interesting possibility (Fig. 9). There are years prior to the early 1990s when wind stress appears to have a clear effect on the timing of the spring stratification and bloom (e.g. the later timings in 1977, 1979 and 1986 associated with stronger spring wind stress), but the variance of the spring wind stress has dropped considerably since the early 1990s. The spring air temperature, however, shows an increasing trend through the 30 years ($0.04\,^{\circ}\mathrm{C\,a^{-1}}$, $r^2 = 0.31$, significant at 99%) with a marked increase at 1990. The length of the time series is just long enough to allow a statistically useful comparison of conditions pre- and post-1990. Before 1990 there is no significant correlation between stratification and bloom timing and the mean spring air temperature, but a significant positive correlation with mean spring wind stress ($r^2 = 0.32$, $n = 17$, significant at 95%). Conversely after 1990 there is no correlation between the timings of stratification and spring bloom and the mean spring wind stress, but correlation with the mean spring air temperature has become significant ($r^2 = 0.33$, $n = 13$, significant at 95%). This analysis indicates that the driving meteorology of the North Sea in spring changed around the early 1990s, from wind stress control, to a reduction in the wind stress and an increase in the influence of the gradually rising air temperature. The time series here is not long enough to assess whether this behaviour is part of a longer period cyclicity in the North Sea climate, or a more sustained change.

Finally, how are these controlling meteorological parameters associated with what is thought to be the key climatic influence of the region, the NAO? Changes in oceanographic conditions in the North Sea have been linked to the NAO (e.g. Becker and Pauly, 1996), as have changes in the North Sea ecosystem (e.g. Fromentin and Planque, 1996). Considering spring wind stress and spring air temperature as the main controls on the timing of stratification and the spring bloom, there is a consistent correlation between wind stress and the spring NAO (Fig. 10a), but no significant correlation between spring air temperature and the spring NAO (Fig. 10b). The wind stress correlation with the NAO is persistent, being significant both pre- and post-1990, while the air temperature correlation with the NAO is not significant either before or after 1990. These correlations were calculated using a spring NAO index defined as the mean NAO index through March, April and May. Separate correlations between spring air temperature and the individual March and April NAO indices showed no significance. A correlation was found between the winter NAO index (December–March) and the mean spring air temperature ($r^2 = 0.17$, $n = 30$,

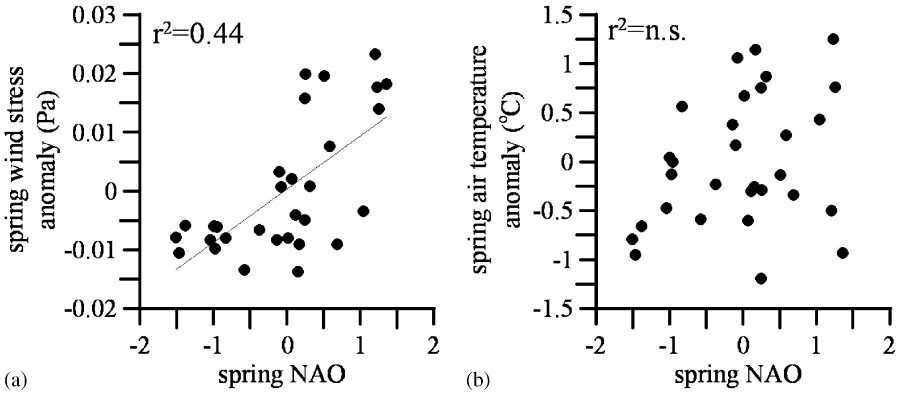

Fig. 10. (a) Linear correlation between the average spring wind stress and the spring NAO index. The correlation is significant at 99% and (b) linear correlation between the average spring air temperature and the spring NAO index. There is no significant correlation.

significant at 95%). There was no significant correlation between the winter NAO index and the spring wind stress. Thus the NAO can directly influence the timing of stratification and the spring bloom through changes in the spring wind stress, but a recent (post-1990) change to a dominant control by spring air temperature has led to a much weaker link to the NAO, probably via changes in winter Atlantic surface water temperatures and their later warming of spring air masses as they move towards the North Sea.

6. Conclusions

In summary, a 1D model successfully hindcast the winter temperature of the north-western North Sea in the vicinity of Marr Bank over the period 1974–2003. The exclusion of any advective inflows to the model heat budget shows that inflows from the north-east Atlantic Ocean do not affect the water temperature. While our study was focussed on a small region of the North Sea off eastern Scotland, this is an effective warning when using water temperature as an indicator of Atlantic inflows (e.g. Reid et al., 2001a). Temperature is unlikely to be a good proxy for oceanic inflows if the slow mean transport of the water from the shelf edge allows the water to reach a local balance with the seasonal meteorology. Evidence for oceanic influences needs to be sought in other, perhaps more direct measurements of cross-shelf edge transport and subsequent advection into the North Sea. The model results confirm that spring stratification occurs on average 1 month after the onset of net surface heating, with the additional time required to increase the heat supply enough to counter the mean tidal mixing. Inter-annual variability of the timing of the spring stratification and bloom is partly linked to the phase of the spring-neap tidal cycle, with established stratification generally beginning as tidal currents decrease towards neaps. The spring-neap cycle can also introduce double-peaked stratification-bloom events. Meteorological forcing of inter-annual variability of the spring stratification and bloom appears to be dominated by changes in the mean spring air temperature. However, despite the short time series, there is evidence in the model results that prior to the early 1990s the spring wind stress (strongly correlated with the NAO) was dominant in the control of the timing variance, while since the early 1990s control has shifted to the mean spring air temperature. The weak correlation between spring air temperature and the NAO indicates that the timing of spring stratification and the bloom may have recently been de-coupled form this basin-scale atmospheric cycle.

It is worth emphasising that we were limited to the period 1974–2003 by the available meteorological data. Over that period the NAO index was predominantly positive, with only a few negative excursions. A greater range of NAO variability, with a time series extending back to 1950 for instance, may lead to stronger correlations between the NAO index and meteorological variables. Similarly, a longer data set would be useful in assessing if the apparent switch in the controlling meteorological parameter about 1990 is unique or occurs periodically. As is often the case, our limited data set does not allow us to separate the effects of a changing climate from those of a varying climate.

Acknowledgements

This work was funded by the European Commission project "Interactions between the marine environment, predators and prey: implications for sustainable sandeel fisheries (IMPRESS; QRRS 2000-30864). Meteorological data was supplied by the British Atmospheric Data Centre. We would also like to thank Fishery Research Services Marine Laboratory Aberdeen, in particular John Dunn, Chris Hall, Mike Heath, Steve Hay, Gayle Holland, Sarah Hughes, George Slesser, and the crew of RV Clupea for their support in the collection and analysis of the mooring data. NAO data came from the Climatic Research Unit, University of East Anglia (http://www.cru.uea.ac.uk/cru/data/nao.htm). We also acknowledge the help gained from the General Ocean Turbulence Model web pages (GOTM: http://www.gotm.net/). We are grateful for the efforts of two anonymous reviewers who helped us to improve the paper.

Appendix A

The numerical model is a 1D model simulating the physics (vertical profiles of currents, turbulence, and temperature) and basic biology (vertical profiles of primary producer biomass and dissolved inorganic nitrogen) of a shelf sea water column. The biological model is identical to that of Sharples and Tett (1994); values of the driving parameters are listed in Table A1. Here we summarise the physical component of the model which is significantly

Table A1
Parameters and their values used in all model runs. Parameter names for the biological model follow Sharples and Tett (1994)

Parameter	Symbol	Value and units
Total water column depth	h	60 m
Depth resolution	Δz	1 m
Time step	Δt	5 s
Latitude	–	56°N
Bottom drag coefficient	k_b	0.0025
Critical Richardson number	Ri_c	0.85
Internal wave eddy viscosity	N_z^{iw}	$1\times10^{-5}\,m^2\,s^{-1}$
Internal wave eddy diffusivity	K_z^{iw}	$1\times10^{-5}\,m^2\,s^{-1}$
Shear eddy viscosity	N_z^{sh}	$1\times10^{-5}\,m^2\,s^{-1}$
Shear eddy diffusivity	K_z^{sh}	$1\times10^{-5}\,m^2\,s^{-1}$
Minimum turbulent kinetic energy for internal waves	E_{min}	$7\times10^{-6}\,m^2\,s^{-2}$
Heat attenuation coefficient	λ	$0.11\,m^{-1}$
PAR attenuation coefficient	λ_0	$0.09\,m^{-1}$
Chlorophyll shading of heat and PAR	ε	$0.012\,m^2\,(mg\,chl)^{-1}$
Seabed nitrogen concentration	S_b	$7.0\,mmol\,m^{-3}$
Seabed nitrogen flux	f_r	$5\,mmol\,m^{-2}\,day^{-1}$
Maximum growth rate	μ_m	$1.2\,day^{-1}$
Quantum yield	α	$4.0\,mg\,C\,(mg\,chl)^{-1}\,day^{-1}\,(W\,m^{-2})^{-1}$
Respiration rate	r^B	$3.0\,mg\,C\,(mg\,chl)^{-1}\,day^{-1}$
Chl:C	q^{chl}	$0.04\,mg\,chl\,(mg\,C)^{-1}$
Maximum nitrogen uptake rate	u_m	$2.0\,mmol\,(mg\,chl)^{-1}\,day^{-1}$
Subsistence cell quota	k_Q	$0.2\,mmol\,mg^{-1}$
Maximum cell quota	Q_m	$1.0\,mmol\,mg^{-1}$
Half-saturation quota	k_u	$0.3\,mmol\,mg^{-1}$
Grazing impact parameter	G	$0.12\,day^{-1}$
Proportion of recycled grazed phytoplankton nitrogen	e	0.5

modified from Sharples and Tett (1994), and Sharples (1999). The model vertical grid, over a total water depth h (m), is split into N equal depth cells of thickness $\Delta z = h/N$. For all model runs presented in this paper the vertical resolution of the model was $\Delta z = 1$ m. The core of the physics component of the model is the integration of the equation of motion:

$$\frac{\partial u}{\partial t} = -g\sum_{i=1}^{m} A_{ix}\cos(\omega_i t - \phi_{ix}) + fv + \frac{\partial}{\partial z}\left(N_z\frac{\partial u}{\partial z}\right), \tag{A.1}$$

$$\frac{\partial v}{\partial t} = -g\sum_{i=1}^{m} A_{iy}\cos(\omega_i t - \phi_{iy}) - fu + \frac{\partial}{\partial z}\left(N_z\frac{\partial v}{\partial z}\right) \tag{A.2}$$

with u and v ($m\,s^{-1}$) the x and y components of velocity, z the vertical co-ordinate (positive upwards), and t (s) is time. The x direction is aligned along the major axis of the M_2 tidal current ellipse as defined by the mooring observations, and the y direction is aligned with the minor axis. The first term on the left of Eqs. (A.1) and (A.2) represents the barotropic tidal forcing of a total of m tidal constituents. For the ith constituent, angular frequency ω_i (s^{-1}), A_{ix} and A_{iy} are the amplitudes of the oscillating sea surface slopes in the x and y directions, and ϕ_{ix} and ϕ_{iy} are the phases of the slope oscillations; $g = 9.81\,m\,s^{-2}$ is the gravitational acceleration. For each tidal constituent the slope amplitudes are calculated from

$$A_{ix} = \frac{C_i}{g}(\omega_i + \lambda_i f); \quad A_{iy} = \frac{C_i}{g}(f + \lambda_i\omega_i) \tag{A.3}$$

with C_i ($m\,s^{-1}$) the length of the semi-major axis of the tidal current ellipse, λ_i is the polarisation of the tidal current ellipse, and f (s^{-1}) is the Coriolis parameter. The semi-major axis and ellipse polarisations were calculated for each tidal constituent following Souza and Simpson (1996). The second term on the left of Eqs. (A.1) and (A.2) is the Coriolis term. Most of the terms of Eqs. (A.1) and (A.2) are integrated implicitly, while the Coriolis term is integrated semi-implicitly, conserving inertial energy (Espelid et al., 2000). The last term on

the right of Eqs. (A.1) and (A.2) described vertical frictional coupling within the water column, with N_z ($m^2\,s^{-1}$) a depth- and time-dependent coefficient of vertical eddy viscosity, calculated by the turbulence closure scheme. A quadratic stress condition is applied at the seabed,

$$\tau_{bx} = -k_b\rho_1\sqrt{(u_1^2+v_1^2)}u_1, \tag{A.4}$$

$$\tau_{by} = -k_b\rho_1\sqrt{(u_1^2+v_1^2)}v_1, \tag{A.5}$$

where τ_{bx} and τ_{by} ($N\,m^{-2}$) are the stresses in the x and y directions, k_b is the bottom quadratic drag coefficient, ρ_b ($kg\,m^{-3}$) is the water density in the bottom model grid cell, and u_1 and v_1 are the current components 1 m above the seabed. A stress is also applied at the sea surface, driven by surface winds, via

$$\tau_{sx} = -c_D\rho_a\sqrt{(u_w^2+v_w^2)}u_w, \tag{A.6}$$

$$\tau_{sy} = -c_D\rho_a\sqrt{(u_w^2+v_w^2)}v_w, \tag{A.7}$$

where τ_{sx} and τ_{sy} ($N\,m^{-2}$) are the surface stresses in the x and y directions, $\rho_a = 1.3\,kg\,m^{-3}$ is the air density, and u_w and v_w are the components of the wind velocity ($m\,s^{-1}$). The reference frame of the wind velocity is rotated so that the wind direction is correct relative to its orientation with the tidal current ellipse. The surface drag coefficient, c_D, is related to the wind speed, w, by (Smith and Banke, 1975)

$$c_D = (0.63 + 0.066w)\rho_s^{-1} \tag{A.8}$$

with ρ_s the surface water density.

Solar irradiance, Q ($W\,m^{-2}$), was available as daily mean values from the meteorological stations. Daily variation of solar irradiance was calculated based on the sunrise and sunset times for the day of the year, with a half-sinusoid variation of instantaneous irradiance between sunrise and sunset and maintaining the mean from the meteorological data. To simulate the rapid attenuation of the red portion of the incident irradiance spectrum, 55% of the incident irradiance is absorbed within the top depth cell of the model. The remaining 45% is then distributed exponentially through the water column according to:

$$\frac{\partial Q_h}{\partial z} = -Q_h(\lambda_0 + \varepsilon_X X) \tag{A.9}$$

with Q_h the local irradiance ($W\,m^{-2}$), λ_0 (m^{-1}) is the heat attenuation coefficient, X is the local concentration of chlorophyll biomass ($mg\,chl\,m^{-3}$), and ε_X is the pigment absorption cross-section ($m^2\,(mg\,chl)^{-1}$).

Heat loss, q_l ($W\,m^{-2}$), from the sea surface is calculated as a function of sea surface temperature (T_s, °C), air temperature (T_a, °C), relative humidity (r_h, %), air pressure (p_a, mb), wind speed and cloud cover (c, %) following Gill (1982) (see also Holt and James, 1999),

$$q_l = h_l + s_k + s_{ke} \tag{A.10}$$

with h_l the long wave radiation, s_k the sensible heat flux, and s_{ke} the evaporative heat flux. The saturated vapour pressure of water, e_w (mb), is related to the sea surface temperature by

$$\log_{10} e_w = \frac{0.7859 + 0.03477T_s}{1.0 + 0.00412T_s} \tag{A.11}$$

with the vapour pressure of water, e_a, then calculated as

$$e_a = 0.01r_he_w \tag{A.12}$$

and the specific humidities of air at sea temperature and at air temperature are, respectively,

$$q_w = \frac{0.62e_w}{p_a - 0.38e_w}, \quad q_a = \frac{0.62e_a}{p_a - 0.38e_a}. \tag{A.13}$$

The heat loss terms in Eq. (A.10) are then given by

$$h_l = e_m\sigma((T_s+273.15)^4)(0.39 - 0.05e_a^{0.5}) \times (1.0 - 0.6c^2\times10^{-4}) \tag{A.14a}$$

(emissivity $e_m = 0.985$; Stefan's constant $\sigma = 5.67\times10^{-8}\,W\,m^{-2}\,K^{-4}$),

$$s_k = c_h\rho_a c_{pa} w(T_s - T_a) \tag{A.14b}$$

(Stanton number $c_h = 1.45\times10^{-3}$; specific heat capacity of air $c_{pa} = 1004.0\,J\,kg^{-1}\,K^{-1}$),

$$s_{ke} = c_e\rho_a w(q_w - q_a)t_l \tag{A.14c}$$

(Dalton number $c_e = 1.5\times10^{-3}$; latent heat $t_l = 2.5\times10^6 - 2.3\times10^3T_s\,J\,kg^{-1}$).

The cloud cover was not available from the meteorological observations, but was instead calculated as a function of the observed mean daily irradiance and the clear sky daily mean irradiance at the sea surface, Q_0, for the time of year at the

latitude of the moorings:

$$Q = Q_0(1 - 0.01 c_f c - 0.38 \times 10^{-4} c^2) \quad \text{(A.15)}$$

with the cloud cover coefficient, c_f, taken to be 0.4.

After the heating has been applied it is redistributed by turbulent mixing within the water column using

$$\frac{\partial T}{\partial t} = \frac{\partial}{\partial z}\left(K_z \frac{\partial T}{\partial z}\right) \quad \text{(A.16)}$$

with K_z ($m^2 s^{-1}$) the depth- and time-dependent coefficient of vertical eddy diffusivity.

The vertical profiles of eddy viscosity and eddy diffusivity are calculated, at each time step of the model, as functions of local current shear and density stratification using the k–ε turbulence scheme of Canuto et al. (2001). The scheme is based on two governing equations for turbulent kinetic energy (E ($m^2 s^{-2}$)) and turbulent dissipation (ε ($m^2 s^{-3}$)):

$$\frac{\partial E}{\partial t} - \frac{\partial}{\partial z}\left(N_z \frac{\partial E}{\partial z}\right) = N_z \Sigma^2 - K_z N^2 - \varepsilon, \quad \text{(A.17)}$$

$$\frac{\partial \varepsilon}{\partial t} - \frac{\partial}{\partial z}\left(N_\varepsilon \frac{\partial \varepsilon}{\partial z}\right) = \frac{\varepsilon}{E}(c_1 N_z \Sigma^2 - c_3 K_z N^2 - c_2 \varepsilon) \quad \text{(A.18)}$$

with

$$\Sigma^2 = \left(\frac{\partial u}{\partial z}\right)^2 + \left(\frac{\partial v}{\partial z}\right)^2, \quad \text{(A.19)}$$

$$N^2 = -\left(\frac{g}{\rho}\frac{\partial \rho}{\partial z}\right), \quad \text{(A.20)}$$

$$c_1 = 1.44, \quad c_2 = 1.92,$$
$$c_3 = \begin{cases} -0.629, & K_z N^2 \geqslant 0, \\ 1, & K_z N^2 < 0, \end{cases} \quad \text{(A.21)}$$

$$N_\varepsilon = \frac{N_z}{1.08}. \quad \text{(A.22)}$$

The turbulent kinetic energy and turbulent dissipation are related via a macro turbulent lengthscale, L (m), through

$$\varepsilon = (c_\mu^0)^3 \frac{E^{3/2}}{L} \quad \text{(A.23)}$$

with $c_\mu^0 = 0.5562$.

Following the law of the wall the boundary conditions for E are

$$E = \left(\frac{u_b}{c_\mu^0}\right)^2 \text{ at } z = 0 \quad \text{and} \quad E = \left(\frac{u_s}{c_\mu^0}\right)^2 \text{ at } z = h, \quad \text{(A.24)}$$

where u_b and u_s are the bottom and surface friction velocities. Boundary conditions for ε are calculated from Eq. (A.23) with $L = \kappa z_0$, where $\kappa = 0.41$ (von Karman's constant) and z_0 is the roughness length of the boundary.

Knowing E and ε (and hence L) leads to the calculation of the eddy diffusivity and eddy viscosity via

$$N_z = c_\mu \sqrt{E} L \quad \text{and} \quad K_z = c'_\mu \sqrt{E} L. \quad \text{(A.25)}$$

The stability functions, c'_μ and c_μ, are related to the velocity shear and stratification with

$$c_\mu = \frac{2}{(c_\mu^0)^3} \frac{\lfloor s_0 + s_1(\tau_E N)^2 + s_2(\tau_E \Sigma)^2 \rfloor}{D}, \quad \text{(A.26)}$$

$$c'_\mu = \frac{2}{(c_\mu^0)^3} \frac{\lfloor s_4 + s_5(\tau_E N)^2 + s_6(\tau_E \Sigma)^2 \rfloor}{D}. \quad \text{(A.27)}$$

The turbulent timescale is $\tau_E = 2E/\varepsilon$ and

$$D = d_0 + d_1(\tau_E N)^2 + d_2(\tau_E \Sigma)^2 + d_3(\tau_E N)^4 + d_4(\tau_E N \Sigma)^2 + d_5(\tau_E \Sigma)^4.$$

The s_i and d_i are constants (see Canuto et al., 2001).

The influence of internal mixing at the thermocline is modelled following the scheme of Large et al. (1994). Shear-induced mixing is parameterised as a decreasing function of the gradient Richardson number as the Richardson number increases towards the k–ε model's critical value, $Ri_c = 0.85$. Above the critical Richardson number, the diffusivity and viscosity are driven by internal waves (K_z^{iw} and N_z^{iw}, respectively) and are held constant. The following are applied within the thermocline (identified by noting when the turbulent kinetic energy falls below a critical value, $E_{\min} = 7 \times 10^{-6}\ m^2 s^{-2}$):

$$K_z = K_z^{iw}; \quad N_z = N_z^{iw}; \quad Ri > Ri_c, \quad \text{(A.28a)}$$

$$\left.\begin{aligned} K_z &= K_z^{iw} + K_z^{sh}\left(1 - \left(\frac{Ri}{Ri_c}\right)^2\right)^3 \\ N_z &= N_z^{iw} + N_z^{sh}\left(1 - \left(\frac{Ri}{Ri_c}\right)^2\right)^3 \end{aligned}\right\} 0 < Ri < Ri_c, \quad \text{(A.28b,c)}$$

$$K_z = K_z^{iw} + K_z^{sh}; \quad N_z = N_z^{iw} + N_z^{sh}; \quad Ri < 0. \tag{A.28d}$$

The internal wave coefficients are taken to be $K_z^{iw} = N_z^{iw} = 1 \times 10^{-5}\,\mathrm{m^2\,s^{-1}}$. For the shear-driven mixing coefficients Large et al. (1994), took $K_z^{sh} = N_z^{sh} = 5 \times 10^{-3}\,\mathrm{m^2\,s^{-1}}$, justified by noting that such a value was within the range of maximum diffusivities found within the oceanic seasonal thermocline. In order that the transient stratification events seen in the mooring data were simulated realistically, we found that this was too high and that a better value was $1 \times 10^{-5}\,\mathrm{m^2\,s^{-1}}$. This is not unreasonable, being similar to diffusivities observed in tidally-energetic shelf seas where thermoclines tend to be sharper than those found in the open ocean as a result of mixing by the tidal boundary layer.

Table A1 summarises all of the parameters and their values used by the model.

References

Becker, G.A., Pauly, M., 1996. Sea surface temperature changes in the North Sea and their causes. ICES Journal of Marine Science 53, 887–898.

Bisagni, J.J., 1998. Estimates of vertical heat flux and stratification from Southern Georges Bank, interannual variability, 1985–1995. Continental Shelf Research 20, 211–234.

Burrows, M., Thorpe, S.A., Meldrum, D.T., 1999. Dispersion over the Hebridean and Shetland shelves and slopes. Continental Shelf Research 19, 49–55.

Canuto, V.M., Howard, A., Cheng, Y., Dubovikov, M.S., 2001. Ocean turbulence. Part I: one-point closure model-momentum and heat vertical diffusivities. Journal of Physical Oceanography 31, 1413–1426.

Cushing, D.H., 1982. Climate and Fisheries. Academic Press, London.

Elliott, A.J., Clarke, T., 1991. Seasonal stratification in the northwest European shelf seas. Continental Shelf Research 11 (5), 467–492.

Espelid, T.O., Berntsen, J., Barthel, K., 2000. Conservation of energy for schemes applied to the propagation of shallow-water inertia-gravity waves in regions with varying depth. International Journal for Numerical Methods in Engineering 49, 1521–1545.

Follows, M., Dutkiewicz, S., 2002. Meteorological modulation of the North Atlantic spring bloom. Deep-Sea Research Part 2 49, 321–344.

Frederiksen, M., Wanless, S., Harris, M.P., Rothery, P., Wilson, L.J., 2004. The role of industrial fishery and oceanographic change in the decline of North Sea black-legged kittiwakes. Journal of Applied Ecology 41, 1129–1139.

Fromentin, J.M., Planque, B., 1996. Calanus and environment in the eastern North Atlantic. 2. Influence of the North Atlantic Oscillation on *C. finmarchicus* and *C. helgolandicus*. Marine Ecology Progress Series 134, 111–118.

Gill, A.E., 1982. Atmosphere–Ocean Dynamics. International Geophysics Series, vol. 30, Academic Press, London, 662pp.

Glorioso, P.D., Simpson, J.H., 1994. Numerical modelling of the M2 tide on the northern Patagonian shelf. Continental Shelf Research 14, 267–278.

Head, E.J.H., Harris, L.R., Campbell, R.W., 2000. Investigations on the ecology of *Calanus* spp. in the Labrador Sea. I. Relationship between the phytoplankton bloom and reproduction and development of *Calanus finmarchicus* in spring. Marine Ecology Progress Series 193, 53–73.

Holliday, N.P., Reid, P.C., 2001. Is there a connection between high transport of water through the Rockall Trough and ecological changes in the North Sea? ICES Journal of Marine Science 58, 270–274.

Holt, J.T., James, I.D., 1999. A simulation of the southern North Sea in comparison with measurements from the North Sea Project. Part 1: Temperature. Continental Shelf Research 19, 1087–1112.

Large, W.G., McWilliams, J.C., Doney, S.C., 1994. Oceanic vertical mixing—a review and a model with a non-local boundary layer parameterization. Reviews in Geophysics 32, 363–403.

Lee, J.-Y., Tett, P., Jones, K., Jones, S., Luyten, P., Smith, C., Wild-Allen, K., 2002. The PROWQM physical–biological model with benthic-pelagic coupling applied to the northern North Sea. Journal of Sea Research 48, 287–331.

Loder, J.W., Greenberg, D.A., 1986. Predicted positions of tidal fronts in the Gulf of Maine region. Continental Shelf Research 6, 397–414.

Loder, J.W., Drinkwater, K.F., Oakey, N.S., Horne, E.P.W., 1993. Circulation, hydrographic structure and mixing at tidal fronts: the view from Georges Bank. Philosophical Transactions of the Royal Society, London A 343, 447–460.

Melle, W., Skjoldal, H.R., 1998. Reproduction and development of *Calanus finmarchicus*, *C. glacialis* and *C. hyperboreus* in the Barents Sea. Marine Ecology Progress Series 169, 211–228.

Moll, A., Radach, G., 2003. Review of three-dimensional ecological modelling related to the North Sea shelf system. Part I: models and their results. Progress in Oceanography 57, 175–217.

Pingree, R.D., Maddock, L., Butler, E.I., 1977. The influence of biological activity and physical stability in determining the chemical distributions of inorganic phosphate, silicate and nitrate. Journal of the Marine Biological Association of the UK 57, 1065–1073.

Platt, T., Fuentes-Yaco, C., Frank, K.T., 2003. Spring algal bloom and larval fish survival. Nature 423, 398–399.

Prandle, D., 1998. Global expressions for seasonal temperatures of the sea surface and ambient air—the influence of tidal currents and water depth. Oceanologica Acta 21, 419–428.

Proctor, R., Wright, P.J., Everitt, A., 1998. Modelling the transport of larval sandeels on the north–west European Shelf. Fisheries Oceanography 7, 347–354.

Reid, P.C., Holliday, N.P., Smyth, T.J., 2001a. Pulses in the eastern margin current and warmer water off the north west European shelf linked to North Sea ecosystem changes. Marine Ecology Progress Series 215, 283–287.

Reid, P.C., de Borges, M.F., Svendsen, E., 2001b. A regime shift in the North Sea circa 1988 linked to changes in the North Sea horse mackerel fishery. Fisheries Oceanography 50, 163–171.

Rodhe, J., 1998. The Baltic and Northern Seas: a process-orientated review of the physical oceanography.

In: Robinson, A.R., Brink, K.H. (Eds.), The Sea, vol. 11. Wiley, New York, pp. 699–732.

Sharples, J., 1999. Investigating the seasonal vertical structure of phytoplankton in shelf seas *Progress in Oceanography* (Supplement. S), 3–38.

Sharples, J., Tett, P., 1994. Modelling observations of the seasonal cycle of primary productivity: the importance of short-term physical variability. Journal of Marine Research 52, 219–238.

Simpson, J.H., 1981. The shelf sea fronts—implications of their existence and behaviour. Philosophical Transactions of the Royal Society, London A 302, 531–546.

Simpson, J.H., Hunter, J.R., 1974. Fronts in the Irish Sea. Nature 250, 404–406.

Smith, S.D., Banke, E.G., 1975. Variation of the sea surface drag coefficient with wind speed. Quarterly Journal of the Royal Meteorological Society 101, 665–673.

Souza, A.J., Simpson, J.H., 1996. The modification of tidal ellipses by stratification in the Rhine ROFI. Continental Shelf Research 16, 997–1007.

Svendsen, E., Magnusson, A.K., 1992. Climatic variability in the North Sea. ICES Marine Science Symposia 195, 144–158.

Sverdrup, H.U., 1953. On the conditions for the vernal blooming of phytoplankton. Journal du Conseil 18, 287–295.

Tett, P., 1987. Modelling the growth and distribution of marine microplankton. In: Ecology of Microbial Communities. Cambridge University Press, Cambridge, MA, pp. 387–425.

Townsend, D.W., Cammen, L.M., 1994. Causes and consequences of variability in the timing of spring phytoplankton blooms. Deep Sea Research Part I 41, 747–765.

Townsend, D.W., Cammen, L.M., Holligan, P.M., Campbell, D.E., Pettigrew, N.R., 1994. Causes and consequences of variability in the timing of the spring phytoplankton blooms. Deep-Sea Research Part I 41, 747–765.

Turrell, W.R., 1992. The East Shetland Atlantic inflow. ICES Marine Science Symposia 195, 127–143.

Turrell, W.R., Henderson, E.W., Slesser, G., Payne, R., Adams, R.D., 1992. Seasonal changes in the circulation of the northern North Sea. Continental Shelf Research 12, 257–286.

Verity, P.G., Wassmann, P., Frischer, M.E., Howard-Jones, M.H., Allen, A.E., 2002. Grazing of phytoplankton by microzooplankton in the Barents Sea during early summer. Journal of Marine Systems 38, 109–123.

Waniek, J.J., 2003. The role of physical forcing in initiation of spring blooms in the northeast Atlantic. Journal of Marine Systems 39, 57–82.